10B.4 THE ORIGIN AND DYNAMICS OF BANNER CLOUDS: AN ANALYSIS BASED ON LARGE EDDY SIMULATIONS

Daniel Reinert* and Volkmar Wirth
Institute for Atmospheric Physics, Johannes Gutenberg-University, Mainz, Germany

1 INTRODUCTION

Banner clouds belong to the class of orographic clouds. They are known to occur in high mountain regions when sufficiently moist air flows across steep mountain peaks or quasi 2D ridges. Preferred places of occurrence are e.g. the Matterhorn in the Swiss Alps, Mount Everest, or Mount Zugspitze in the Bavarian Alps. Figure 1a,b shows two typical examples.

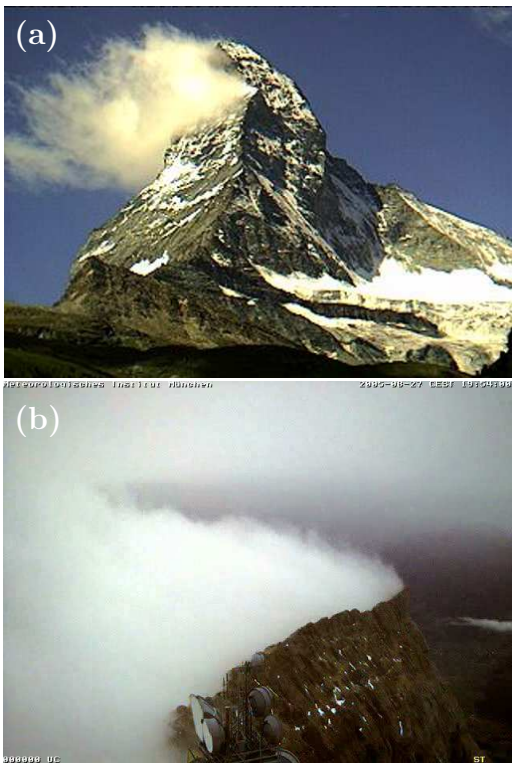

Figure 1: *Banner clouds forming leeward of a pyramidal shaped mountain peak or a quasi 2D ridge. (a) Banner cloud at Matterhorn (Switzerland). (b) Banner cloud at Mount Zugspitze (Bavarian Alps). Mean flow from right to left.*

Banner clouds have the distinction of being confined to the immediate lee of the mountain, whereas the windward side remains cloud-free. They typically have a banner-like appearance with a characteristic horizontal scale of $O(1\,\mathrm{km})$. Usually their upwind end is directly attached to the mountain tip while their downwind end flickers in the wind resembling a flag. Banner clouds are quasi-stationary and can often be observed for several hours. They must be clearly distinguished from other orographically induced cloud patterns like cap clouds, lee wave clouds or rotor clouds. These either form on the windward side due to forced lifting or develop several kilometers downwind of the mountain crest as a result of trapped lee waves.

Banner clouds, despite their regular appearance, were always on the fringe of scientific attention. The underlying mechanism of formation, as well as the relative importance of dynamics versus thermodynamics for formation and maintenance, are not fully understood. Besides a number of drawings and photographs, very few investigations related to banner clouds are documented in the scientific literature. We are aware of early measurements conducted by Peppler (1927) at Säntis (Switzerland) and Joachim Kuettner (1946) (pers. comm.) at Mount Zugspitze. Unfortunately, these measurements still do not provide a complete picture of the phenomenon. The only numerical study we are aware of was conducted by Geerts (1992) using a model based on the Reynolds Averaged Navier-Stokes (RANS) equations. He focused on the relative importance of surface friction for lee upslope flow behind an idealised tetrahedral-shaped obstacle.

In the scientific literature mainly three qualitative arguments are put forth in order to explain the occurrence of banner clouds. According to them the cloud develops due to:

I mixing of cold air near the ground with warmer air from above (i.e. banner clouds being essentially mixing fog) (e.g. Humphreys, 1964)

II local adiabatic cooling near the mountain top due to flow acceleration along quasi horizontal trajectories originating on the windward side (Bernoulli-effect) (e.g. Beer, 1974)

* *Corresponding author address:* Daniel Reinert, Johannes Gutenberg-University, Institute for Atmospheric Physics, Becherweg 21, 55099 Mainz, Germany; e-mail: dreinert@uni-mainz.de

III adiabatic cooling due to forced upwelling in the upward branch of a leeward vortex with horizontal axis (e.g. Douglas, 1928) (see Fig. 2).

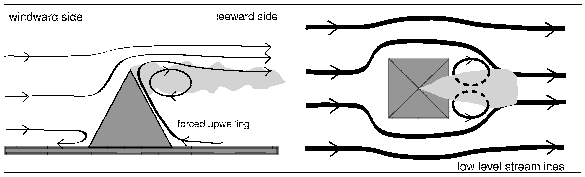

Figure 2: *Schematic, illustrating the postulated formation mechanism of banner clouds leeward of pyramidal shaped mountain peaks according to argument* III. *Left: flow in x-z-plane. Right: low level flow in x-y-plane. Light shading denotes the cloud.*

We believe that argument III is the most relevant one, since it fits best with recent observations taken by us at Mount Zugspitze (Schween et al, 2007). Nevertheless, a distinct proof of argument III based on eddy-resolving numerical simulations is still lacking.

This paper aims at providing more insight into the dynamics of banner clouds with the aid of Large Eddy Simulations (LES). We will clarify the dominant formation mechanism and the necessity of additional leeward moisture sources, radiative effects or distinct air masses. Further we will investigate the relative importance of thermodynamics regaring the reinforcement and maintenance of banner clouds.

2 APPROACH

As a tool to investigate this phenomenon we developed a new LES model which can handle moist atmospheric flow above highly complex terrain (Reinert et al, 2007; Reinert and Wirth, 2008). The model is able to treat orography with slopes up to 90° by applying the method of viscous topography (Mason and Sykes, 1978). Furthermore, turbulent inflow conditions can be generated by using a modified perturbation recycling method (Lund et al, 1998; Reinert and Wirth, 2008). Precipitating clouds are accounted for with a 2-moment warm microphysical bulk scheme. The model has been tested in detail and was validated against wind tunnel data.

Since pyramidal shaped mountains seem to be the most preferred places for banner cloud occurrence, we investigated the flow field around idealised pyramidal shaped obstacles on experimental as well as atmospheric scale. The numerical simulations on experimental scale were also validated against wind tunnel data of Ikhwan and Ruck (2006). Thus more insight could be gained regarding the robustness of our findings for the banner cloud problem.

Figure 3 gives a general idea of the model setup. In x-direction we applied open inflow/outflow boundaries while in y-direction cyclic boundary conditions were used. Since in LES the inflow already needs to comprise realistic turbulent structures, we generated model consistent turbulence in a precursor run by using the perturbation recycling technique. Then, for each time step, slices of the generated turbulent data set were applied at the inflow boundary. Table 1 provides an overview about chosen model parameters, like the horizontal (Δx) and vertical (Δz) resolution, the obstacle shape (edge length L and slope angle α), the velocity of the approaching flow at the top of the domain U_0 and the total number of grid points N_{xyz}.

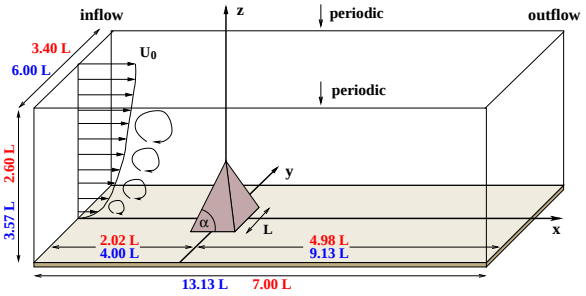

Figure 3: *Model setup on experimental (**blue**) and atmospheric (**red**) scale*

	L [m]	α [°]	Δx [m]	Δz_m [m]	U_0 [ms^{-1}]	N_{xyz} [#]
exp	0.2	70	1.3E-2	9E-3	5.4	$0.91E6$
atm	930	65	25	15	9.0	$2.2E6$

Table 1: *Model parameters for experimental (exp) and atmospheric (atm) scale. L and α are the edge length and slope angle of the obstacle, respectively, Δx is the horizontal and Δz_m the minimum vertical grid spacing (vertically stretched grid), U_0 is the velocity at the top of the domain and N_{xyz} gives the total number of grid points.*

3 RESULTS

3.1 Simulations on experimental scale

On experimental scale the simulations were conducted for a dry, neutrally stratified boundary layer exhibiting a logarithmic velocity profile. The inflow conditions were chosen according to the wind tunnel setup of Ikhwan and Ruck (2006). Figure 4a,b shows statistics of the generated turbulent inflow data set which is applied at the inlet. It can be seen that both the simulated mean velocity profile and the normal stresses (lines) compare well with the wind tunnel results (symbols). This confirms the appropriateness of the applied inflow generation technique.

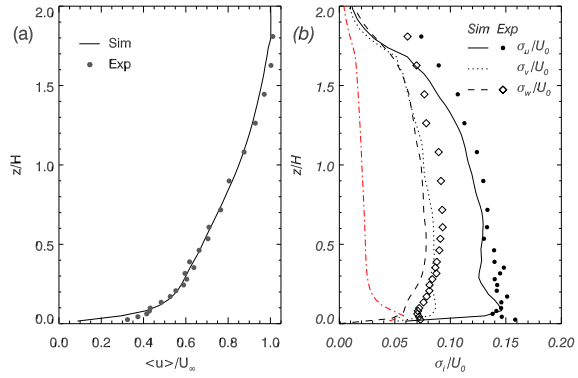

Figure 4: *Statistics of the generated turbulent inflow data set (lines) compared to wind tunnel data (symbols). (a) profile of time averaged horizontal velocity <u>. (b) profiles of normalised total (subgrid + resolved) standard deviations σ_u, σ_v, σ_w. Red line shows subgrid contribution to σ_u.*

Figure 5 shows the simulated time averaged flow field in x-z-plane along the line of symmetry y/H=0. H denotes the pyramid height and the colours show the time averaged vertical velocity <w>. Red colours show upward, blue colours downward motion. The flow is characterised by a recirculation region in the lee with significant upwelling towards the pyramid's tip. Moreover, the flow field is highly asymmetric, i.e. the vertical extent of the upwelling region is much larger on the leeward compared to the windward side. For the latter, air parcels approaching the pyramid at heights lower than the height of the stagnation point X_s are deflected downward. Based on these results, argument III, presented in Sect. 1, seems to apply. Dynamically driven upwelling in the lee may indeed be responsible for banner cloud formation.

Nevertheless, from this Eulerian point of view (Fig. 5) one cannot deduce, whether banner cloud formation is possible even for horizontal homogeneous conditions in terms of temperature and humidity or whether additional leeward moisture sources or air masses with distinct temperatures are a necessary condition. Under horizontally homogeneous conditions, the maximum vertical displacement of air parcels in the lee must exceed the displacement on the windward side. Otherwise asymmetric (i.e. banner-like) cloud formation would not be possible. Simply looking at the vertical extent of the upwelling regions may lead to erroneous conclusions, since the flow field also exhibits significant downwelling along the lateral faces of the pyramid (not shown). Additional Lagrangian-like information is necessary.

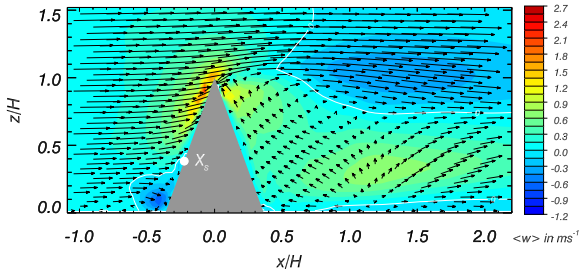

Figure 5: *Simulated time averaged flow on experimental scale along the line of symmetry $y/H = 0$. Colours show the time averaged vertical velocity <w>*

For that reason we additionally advected a passive tracer Φ, satisfying $\mathrm{D}\Phi/\mathrm{D}t = 0$. The tracer was initialised as follows: $\Phi(x_{inlt}, y, z) = z$, i.e. the tracer concentration allocated to each air parcel equals the starting height z of the air parcel at $x = x_{inlt}$, where x_{inlt} denotes the inflow boundary. The time averaged field of vertical air parcel displacement Δz can thus be deduced according to:

$$\Delta z(x, y, z) = \Phi(x_{inlt}, y, z) - < \Phi > \ , \qquad (1)$$

where <Φ> denotes the simulated time averaged 3D-field of Φ. Figure 6a,b shows contours of $\Delta z/H$ in the x-z-plane along the line of symmetry and in the x-y-plane near the pyramid's tip.

It can be seen that the flow field is highly asymmetric regarding the Lagrangian vertical displacement. Air parcels which have been lifted to the top in the upward branch of the induced vortex on

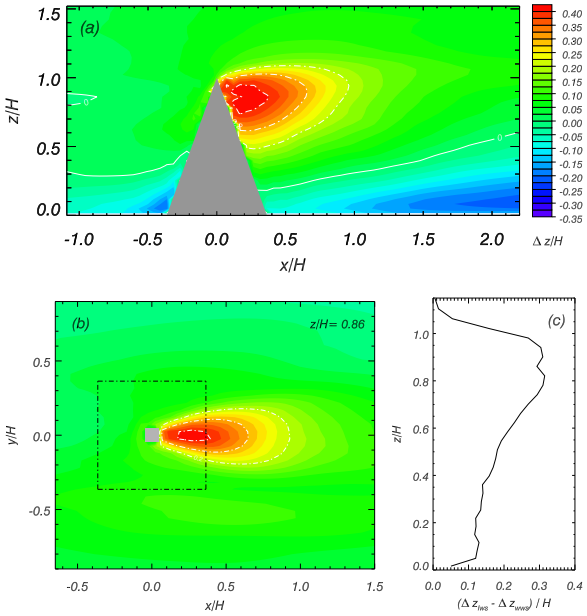

Figure 6: *(a) Time averaged vertical displacement $\Delta z/H$ along the line of symmetry $y/H = 0$. (b) $\Delta z/H$ in an x-y-plane at $z/H = 0.86$. Contours of $\Delta z/H = 0, 0.2, 0.3, 0.4$ are additionally highlighted. (c) Displacement asymmetry $\Delta z_{lws} - \Delta z_{wws}$, parallel to the obstacle slopes at $y/H = 0$.*

the leeward side (lws) originate at lower levels (exhibit larger Δz) than air parcels which have been lifted on the windward side (wws). The asymmetry $\Delta z_{lws} - \Delta z_{wws}$ is largest slightly below the pyramid's tip, as shown in Fig. 6c. This is exactly the place where banner clouds are known to occur. The maximum value of this asymmetry may be regarded as a measure for the probability of banner cloud formation for the given obstacle geometry, since with increasing asymmetry there is a broader range of temperature and humidity profiles which allow asymmetric (i.e. banner-like) cloud formation. We investigated pyramids of various slopes α and heights H and found that this asymmetry increases with increasing height and with increasing slope of the pyramid. This is in agreement with the observation that banner clouds are usually restricted to very high and steep mountain peaks.

Due to the observed strong asymmetry it can be stated that banner clouds may indeed form under horizontally homogeneous conditions in terms of moisture and temperature.

3.2 Simulations on atmospheric scale

In order to provide further evidence, the simulations were repeated on atmospheric scale for a moist boundary layer (BL) with the cloud physics switched on. The model was initialised horizontally homogeneous without any additional leeward moisture sources, distinct air masses or radiative effects. The chosen background profiles of virtual potential temperature θ_v and specific humidity q_v are shown in Fig. 7a.

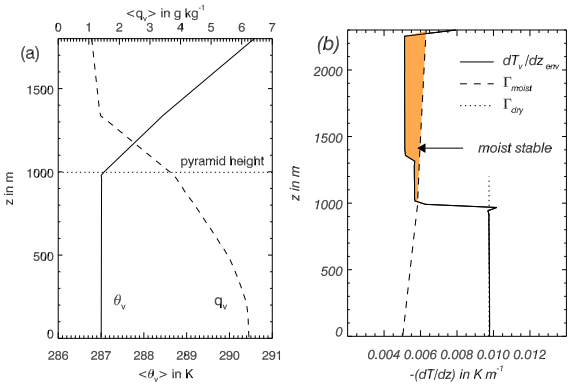

Figure 7: *(a) Environmental profiles of time averaged virtual potential temperature θ_v and specific humidity q_v. (b) Stability analysis for θ_v-profile shown in (a). Γ_{dry} is the dry adiabatic lapse rate, Γ_{moist} is the moist adiabatic lapse rate and $\mathrm{d}T_v/\mathrm{d}z_{\mathrm{env}}$ is the chosen environmental lapse rate.*

These profiles were motivated by measurements which were taken by us at Mount Zugspitze during a banner cloud event. The measurements exhibited a well mixed turbulent BL slightly exceeding mountain peak height and a stable layer aloft. The vertical gradient of θ_v above the turbulent BL was chosen such that the atmosphere was unconditionally (moist) stable for $z > 1000\,\mathrm{m}$. This is illustrated in the stability analysis of Fig. 7b. For $z > 1000\,\mathrm{m}$ the moist adiabatic lapse rate Γ_{moist} exceeds the environmental lapse rate $\mathrm{d}T_v/\mathrm{d}z_{\mathrm{env}}$ which is indicative for a moist stable atmosphere. Without a moist stable layer aloft, triggering of clouds in the lee would lead to convection, significantly exceeding mountain peak height. As suggested in Schween et al (2007), we exclude predominantly convective clouds from the species of banner clouds. The absolute values of θ and q_v were chosen to yield Lifting Condensation Levels (LCL) which are below obstacle height H for large parts of the boundary layer depth. This is of course a

necessary condition for banner cloud occurrence. The mean profile of horizontal velocity $<u>$ again was chosen to be logarithmic up to $z = H$ with a constant value of $U_0 = 9\,\mathrm{ms}^{-1}$ above. Turbulent inflow data based on these mean profiles were again created in a precursor run.

Figure 8 shows a snapshot of the simulated cloud structures. The cloud is visualised by an isosurface of the cloud water content $q_c = 0.01\,\mathrm{gkg}^{-1}$ and coloured with the instantaneous vertical velocity. The cloud strongly resembles naturally occurring banner clouds. Except for some pieces of cloud which occur on the windward side as a result of boundary layer turbulence, the cloud is almost entirely confined to the lee and is directly attached to the upper part of the mountain. The colours indicate strong upwelling in the immediate lee and downwelling about one obstacle height downwind. Figure 9 shows the corresponding time averaged cloud water content along the line of symmetry $y = 0\,\mathrm{m}$. Once again, the typical banner cloud shape is apparent.

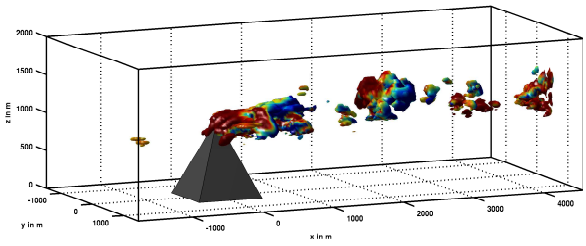

Figure 8: *Snapshot of simulated cloud structures visualised by an isosurface of the specific cloud water content ($q_c = 0.01\,\mathrm{gkg}^{-1}$). Colours show instantaneous vertical velocity w. Red colours show upwelling, blue colours downwelling.*

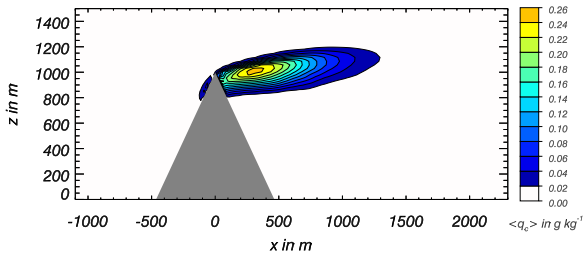

Figure 9: *Time averaged cloud water content along the line of symmetry $y = 0\,\mathrm{m}$.*

The fact that we are able to numerically reproduce banner-like cloud structures which strongly resemble naturally occurring ones, strongly suggests that this experiment captures the main mechanism of formation. This strongly supports argument III, since all other mechanisms under discussion, including local adiabatic cooling due to the *compressible* Bernulli-effect, have been excluded from this simulation. Furthermore, this simulation clearly shows that, at least for pyramidal shaped mountain peaks, there is no need for additional leeward moisture sources, radiative effects or distinct air masses in order for banner clouds to form.

3.3 Impact of moisture physics

As shown in Fig. 10, in situ measurements were conducted at Mount Zugspitze in order to characterise the air masses on both sides of the ridge.

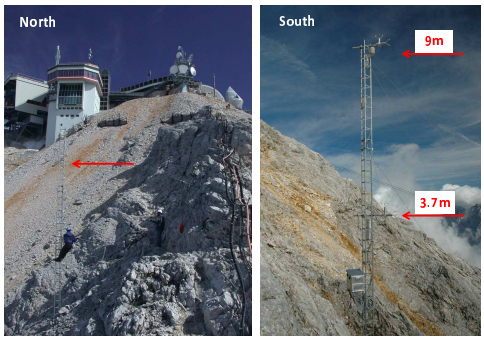

Figure 10: *Measuring poles located northern and southern to the tip of Mount Zugspitze.*

Figure 11a,b shows timeseries of temperature and specific humidity measured at the poles during the 16.10.2008. The solid and dashed lines show measurements at the leeward (northern) and windward (southern) side, respectively. During that day a banner cloud was observed on the northern side. The corresponding time span is shaded in gray. It can be seen that during the banner cloud event the air in the lee was about 1.5 K warmer and $0.5\,\mathrm{gkg}^{-1}$ moister than the air on the windward side (the additional cloud liquid water q_c is not taken into account). This is in accordance with the measurements conducted by Joachim Küttner in 1946 (pers. comm.); the reason for the observed differences on windward versus leeward side was unclear. Differences in temperature may result from:

- radiative effects or heating of leeward air due to contact with the ground

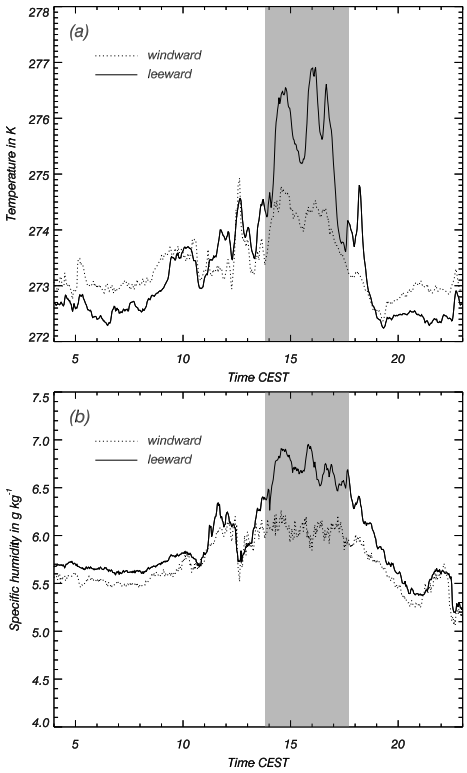

Figure 11: *Timeseries of (a) temperature T and (b) specific humidity q_v at Mount Zugspitze for the windward (dashed) and leeward (solid) side. Gray shading denotes time span during which a banner cloud was observed.*

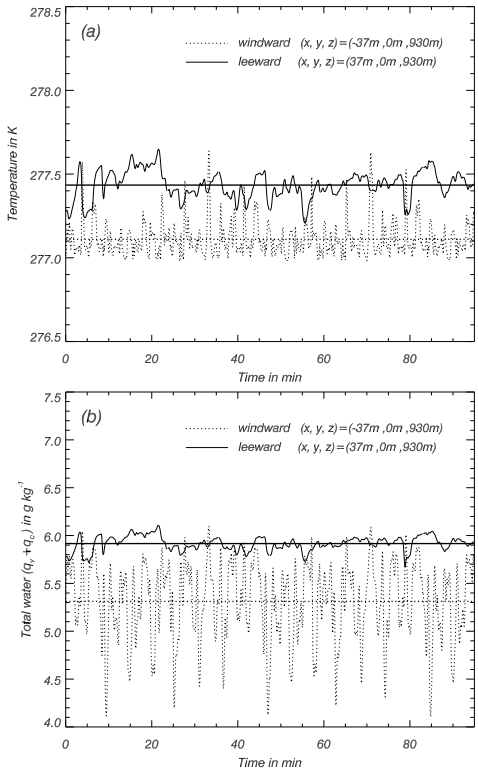

Figure 12: *Timeseries of (a) temperature T and (b) total water (q_v+q_c) next to the pyramid's tip as taken from the numerical simulation. Dashed line: windward side; Solid line: leeward side. Thick lines indicate time averages.*

- latent heat release

The observed differences in specific humidity could be due to:

- additional leeward moisture sources at the ground (such as lake *Eibsee* in the valley to the north)
- distinct air masses on windward versus leeward side with different origins
- larger vertical displacement of air parcels on leeward compared to the windward side

For qualitative comparison, Fig. 12 shows time series of T and $q_t = q_v + q_c$ as derived from our numerical simulations. The selected points are located on the windward and leeward side next to the pyramid's tip (see Fig. 12 for exact positions). It can be seen, that the model is able to qualitatively reproduce the measurements at Mount Zugspitze. The air on the leeward side is about 0.3 K warmer and about 0.6 gkg^{-1} moister than the air on the windward side. For the numerical simulation these differences can be explained as follows: Since the oncoming turbulent BL was chosen to be almost neutrally stratified, the differences in temperature can purely be ascribed to leeward condensation and corresponding latent heat release. The differences in q_t result from differences in the Lagrangian vertical displacement on windward versus leeward side (specific humidity typically decreases with increasing distance from the ground, as given in Fig. 7a). Thus in order to qualitatively explain the observations at Mount Zugspitze, explanations involving radiative effects, distinct air masses or additional leeward moisture sources are not necessary. Nevertheless, due to the observed quantitative differences it can not be ruled out that for quasi-2D ridges like Mount Zugspitze other effects, like those mentioned above, play an additional role.

Our simulations suggest that the differences in temperature and humidity, as observed on Mount Zugspitze, should be a common feature of banner

clouds. While differences in moisture are induced by the dynamics, the differences in temperature are a result of moisture physics.

From the observed and simulated differences the following consequence results: Since the relatively dry and cold air on the windward side is forced to flow over the warmer and moister air on the leeward side, banner clouds give rise to a destabilisation of the lee near the mountain's tip. This is illustrated in Fig. 13a, where modelled vertical profiles of the Brunt-Väisälä frequency

$$N^2 = \frac{g}{\theta_v}\frac{\partial \theta_v}{\partial z} \qquad (2)$$

are shown for the immediate lee. The thick solid line shows results from the full simulation, as presented in Sect. 3.2 (here referred to as *moist run*). In a saturated atmosphere the moist Brunt-Väisälä frequency N_m^2 (Durran and Klemp, 1982) is probably a better representation of the actual static stability. For the cloudy region (gray shaded) this parameter is given by the dashed line. It can be seen that the effective Brunt-Väisälä frequency is lower when the atmosphere is saturated than when it is dry. To explicitly determine the importance of moist physics (i.e. latent heat release) this model run was reconducted with the source terms in the θ-equation switched off (here referred to as *dry run*). Thus the effect of latent heat release/consumption onto the dynamics was neglected. The resulting N^2-profile is given by the dotted line.

For the moist run, the N^2-profile exhibits a dipole-like structure with positive values for $770\,\mathrm{m} < z < 1120\,\mathrm{m}$. Thus compared to the dry run, the atmosphere is stabilised within the lower part of the cloudy region, while the upper part is destabilised and is even statically unstable on average. When considered in terms of the moist Brunt-Väisälä frequency N_m^2, the destablizing effect is even larger.

The observed dipole in N^2 should impact leeward turbulence. Regions with $N^2 < 0$ should give rise to buoyant production of turbulence while regions with $N^2 > 0$ should give rise to a negative contribution to the TKE budget (in terms of the buoyant production term). Figure 13b shows vertical profiles of the total TKE for the moist (solid line) and dry (dotted line) run. These profiles were derived by averaging over the region $487\,\mathrm{m} < x < 937\,\mathrm{m}$. The TKE-profiles show similar shapes, indicating that most of the leeward turbulence was generated mechanically in both runs, associated with flow separation. The

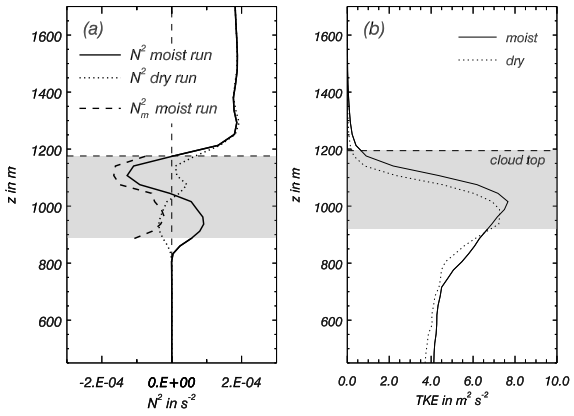

Figure 13: *(a) time and space averaged vertical profiles of the Brunt-Väisälä frequency N^2 (solid line) and its moist counterpart N_m^2 (dashed line) in the mountain's lee (space averaged for $237\,\mathrm{m} < x < 687\,\mathrm{m}$ at $y = 0\,\mathrm{m}$) for the moist run. The dotted line shows N^2 for the dry run. (b) time and space averaged vertical profiles of resolved TKE for the moist and dry run (space averaged for $487\,\mathrm{m} < x < 937\,\mathrm{m}$ at $y = 0\,\mathrm{m}$). Vertical extent of the cloud (moist run) is shaded in gray.*

maxima of both profiles coincide with the vertical position of the separating shear layer. The buoyant generation/decay of leeward turbulence seems to be of secondary importance. Nevertheless, consistent with the N^2-profiles shown in Fig. 13a, TKE is enhanced in the moist run for the altitude range with $N^2 < 0$. Likewise, the comparatively low values of TKE for the moist run in the region $900\,\mathrm{m} < z < 1000\,\mathrm{m}$ could be a manifestation of the positive N^2-anomaly apparent in Fig. 13a. Furthermore the vertical position of those low TKE values agrees well with the vertical position where N_m^2 slightly exceeds N^2 for the dry run. We verified that the observed differences in TKE far below the cloudy region do not result from differences in the TKE-profiles upstream of the mountain peak; although intermittent cloud development can also be observed far upstream of the mountain within the oncoming boundary layer, differences in the upstream TKE-profiles are negligible. Thus the slightly enhanced TKE far below the cloudy region (moist run) must be a result of the moist physics, too.

Apart from the influence on leeward TKE, one could imagine that moist physics also have the potential to reinforce or sustain the upward branch of the leeward vortex which could help to sustain banner clouds during episodes with minor dynam-

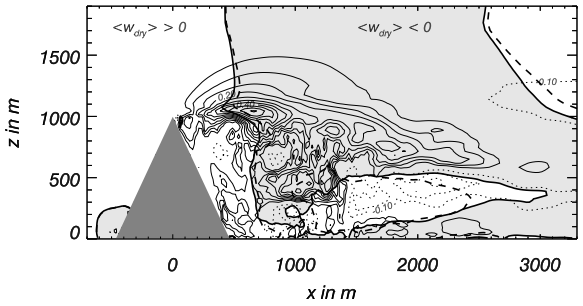

Figure 14: *Contours of* $<\Delta w>=<w_{\mathrm{moist}}>-<w_{\mathrm{dry}}>$ *along* $y = 0\,\mathrm{m}$, *showing differences between the time averaged vertical velocity for the moist and dry run, respectively. Contour interval:* $0.05\,\mathrm{ms}^{-1}$. *Solid lines show* $<\Delta w> > 0$. *The zero line is omitted. The solid and dashed thick lines distinguish regions with up- and downwelling for the dry and moist run, respectively. The shading highlights areas with downward motion for the dry run.*

ical forcing. In order to estimate the impact of moist physics on the mean flow, we compared time averaged fields of vertical velocity $<w>$ along the line of symmetry $y = 0\,\mathrm{m}$. Figure 14 shows contours of $<\Delta w>=<w_{\mathrm{moist}}>-<w_{\mathrm{dry}}>$ which is the difference in $<w>$ between the moist and dry run, respectively. For the dry run, in addition, regions with upward and downward motion are separated by the thick solid line. Regions with downward motion are shaded in gray. Correspondingly, the thick dashed line separates up- and downwelling regions for the moist run. While differences between those thick lines provide some information about structural differences regarding the position and shape of up- and downwelling regions, the contours emphasise its absolute change in strength.

As can be seen, structural differences between the moist and the dry run are small. Differences are somewhat more pronounced regarding the strength of the up- and downwelling regions. The downward directed branch of the secondary circulation is weakened for the moist run, which is indicated by a positive $<\Delta w>$ in Fig. 14 within the gray shaded region. This is of course directly related to latent heat release during cloud formation which counteracts the dynamically forced downwelling in this region. On the other hand, latent heat release barely impacts the strength of the upward branch of the secondary circulation. For the moist run, the upward branch is only slightly enhanced nearby the mountain's tip and its foot. This enhancement is far to small for being an effective process to systain banner clouds when dynamical forcing breaks down. Overall, there is a much stronger impact on the downward- compared to the upward branch. This is embodied in the change of the maximum positive and negative vertical velocities. Relative to the dry run, the maximum vertical velocity in the upward branch hardly changes, while the maximum vertical velocity in the downward branch decreases about 11%.

4 CONCLUSIONS

This paper aims at providing more insight into the origin and dynamics of orographically induced banner clouds. We numerically investigated air flow around idealised pyramidal shaped obstacles on both experimental and atmospheric scale, including model runs with moisture physics switched on and off. We were able to present the first LES of a realistically shaped banner cloud. The simulations provide evidence that banner clouds are predominantly a dynamical phenomenon. They form due to dynamically forced upwelling and adiabatic cooling in the upward branch of a secondary leeward circulation. Since the flow field was found to be highly asymmetric regarding the Lagrangian vertical displacement on leeward versus windward side, banner cloud formation was even possible for horizontally homogeneous conditions regarding both moisture and temperature. These results lead us to conclude that additional leeward moisture sources, distinct air masses and radiation effects are no necessary condition for banner cloud formation. This contradicts earlier explanations given in classical textbooks (e.g. Beer (1974) or Humphreys (1964)), which are based upon Bernoulli- or mixing fog theories.

A comparison of model runs with the cloud model switched on and off indicated that (at least for the thermodynamical situation given in Fig. 7a) thermodynamics (i.e. latent heat release) do not significantly impact the mean flow and are unlikely to significantly reinforce or sustain the flow field giving rise to banner cloud formation. On the other hand, thermodynamics do impact the leeward stratification. Latent heat release leads to a destabilisation of the upper part of the banner cloud which results in a moderate increase of leeward turbulence.

References

Beer T (1974) Atmospheric Waves. Adam Hilger Press

Douglas CKM (1928) Some alpine cloud forms. Quarterly Journal of the Royal Meteorological Society 54:175–178

Durran DR, Klemp JB (1982) On the effects of moisture on the Brunt-Väisälä frequency. Journal of the Atmospheric Sciences 39:2152–2158

Geerts B (1992) The origin of banner clouds: A potential vorticity perspective. Sixth Conference on Mountain Meteorology, Portland, Oregon P1.5:97–98

Humphreys JW (1964) Physics of the air. Fourth Ed.; Dover Publ.

Ikhwan M, Ruck B (2006) Flow and pressure field characteristics around pyramidal buildings. Journal of Wind Engineering and Industrial Aerodynamics 94(10):745–765

Lund TS, Wu XW, Squires KD (1998) Generation of turbulent inflow data for spatially-developing boundary layer simulations. Journal of Computational Physics 140:233–258

Mason PJ, Sykes RI (1978) A simple cartesian model of boundary layer flow over topography. Journal of Computational Physics 28:198–210

Peppler W (1927) Hinderniswolken am Säntisgipfel. Das Wetter 44:212–213

Reinert D, Wirth V (2008) A new LES model for simulating air flow and warm clouds above highly complex terrain. Part II: The moist model and its application to banner clouds. Boundary Layer Meteorology, Under revision

Reinert D, Wirth V, Eichhorn J, Panhans WG (2007) A new LES model for simulating air flow and warm clouds above highly complex terrain. Part I: The dry model. Boundary Layer Meteorology 125:109–132

Schween J, Kuettner J, Reinert D, Reuder J, Wirth V (2007) Definition of 'banner clouds' based on time lapse movies. Atmospheric Chemistry and Physics 7:2047 – 2055, URL www.atmos-chem-phys.net/7/2047/2007/